

High Circular Dichroism in Extrinsic Chiral Metamaterials Based on Sawtooth and Zigzag Arrangements With Experimental Validation

Jihad Ben Yamoun^{1b}, Oscar Fernández^{2b}, Noura Aknin, *Senior Member, IEEE*,
and Álvaro Gómez-Gómez^{2b}, *Member, IEEE*

Abstract—This study analyzes the extrinsic chirality of metamaterials based on printed circuit board (PCB). Inspired by extrinsic planar metamaterials, two novel 3-D chiral metamaterials (CMMs) have been proposed and analyzed. In these structures, called sawtooth and zigzag arrangements, each unit cell and not the entire metamaterial is tilted with respect to the incident field. In both cases, the same single-layer metallic pattern, that is, a split-ring resonator (SRR), was used. In comparison with the traditional planar extrinsic chiral structures, it is shown, by numerical and experimental characterization, that these new types of arrangements exhibit a larger circular dichroism (CD), approximately 0.90, in the X-band, with a significant wideband response. The analysis of the extrinsic chirality shows that it is originated by the dipole moments excited on the unit cells. With circular polarization, the constructive/destructive interference between these dipoles produces CD. However, owing to the broadside coupling between adjacent unit cells, the proposed nonplanar arrangements provide higher CD values than the planar structure.

Index Terms—Chirality, circular dichroism (CD), extrinsic chirality, metamaterials.

I. INTRODUCTION

CHIRAL media have attracted the attention of scientists since Arago noticed in 1811 that quartz could rotate the plane of polarization of light [1], [2]. Chiral particles are found in several disciplines including biology, chemistry, and electromagnetics. From a geometrical point of view, they present the particularity that cannot be superimposed with its mirror image by means of rotation or translation in a plane. From an electromagnetic point of view, this characteristic provides different refractive indices for right- and left-handed circularly polarized waves (RCP and LCP, respectively), resulting in interesting properties, such as circular birefringence

and circular dichroism (CD). In natural chiral media, these properties are very low in magnitude. However, this drawback can be overcome using chiral metamaterials (CMMs). In general, metamaterials are artificial media that can provide electromagnetic properties that are not usually found in natural materials or, at least, not with a high magnitude [1]. The subset of CMM can provide high optical activity or CD with a small thickness [3]. In fact, CMM represent an alternative route for obtaining negative refraction without simultaneous negative permittivity and permeability [4]. Many works available in the literature [5], [6], [7], [8], [9], [10], [11], [12], [13] have proposed and studied microwave and optical CMM, from bulk 3-D CMMs to planar chiral metasurfaces. CMM can be applied, for example, to design antenna superstrates to modify the antenna performance, its gain [14], [15], [16], or radiation properties [10], [17].

Some authors, such as Plum et al. [18], [19], [20], refer to this chirality due to the geometry of the CMM itself, intrinsic chirality. This terminology is applied to differentiate this type of chirality from that originated by the mutual orientation between the wave propagation direction and the planar metamaterial normal, called extrinsic chirality. The first studies on extrinsic chirality in CMM were presented in [18], [19], and [20]. They showed that a single-layer planar meta-molecule (intrinsically achiral) may exhibit chiral behavior if the incidence is not normal to the structure, even in non-(intrinsically) chiral structures. With this condition, the unit cell, observed from the incident plane wave, behaves as a 3-D chiral structure. This chiral behavior strongly depends on the angle of incidence, α . In [18], CD values of 0.3° and 21° of optical activity were reported with $\alpha = 30^\circ$. In [20] polarization azimuth rotation values of 80° were presented for $\alpha = 10^\circ$. The planar structure presented in [21] exhibited CD values of 0.58 with $\alpha \approx 80^\circ$.

However, the extrinsic chirality depends not only on the geometry of the chiral meta-molecule, but also on how it is distributed along the metamaterial and oriented with regard to the incident wave. In [22], it was analyzed the combination of intrinsic and extrinsic chirality in dual layer rosette structures in zigzag or sawtooth distributions, showing CD values of up to 0.7. In [23], it was studied a zigzag reflective multifunctional metamaterial created by folding a planar metamaterial formed by horizontal metal strips. This work shows absorption

Manuscript received 21 April 2023; accepted 4 June 2023. This work was supported by the MCIN/AEI/10.13039/501100011033/ERDF “A way to make Europe” through the R + D + i Project under Grant PGC2018-098350-B-C22. (Jihad Ben Yamoun and Oscar Fernández are co-first authors.) (Corresponding author: Oscar Fernández.)

Jihad Ben Yamoun and Noura Aknin are with the Physics Department, Faculty of Sciences, University Abdelmalek Essaadi, Tetuan BP 2121, Morocco (e-mail: jihad.benyamoun@etu.uae.ac.ma; noura.aknin@uae.ac.ma).

Oscar Fernández and Álvaro Gómez-Gómez are with the Departamento de Ingeniería de Comunicaciones, Universidad de Cantabria, E39005 Santander, Spain (e-mail: oscar.fernandez@unican.es; alvaro.gomez@unican.es).

Color versions of one or more figures in this article are available at <https://doi.org/10.1109/TMTT.2023.3297273>.

Digital Object Identifier 10.1109/TMTT.2023.3297273

0018-9480 © 2023 IEEE. Personal use is permitted, but republication/redistribution requires IEEE permission.
See <https://www.ieee.org/publications/rights/index.html> for more information.

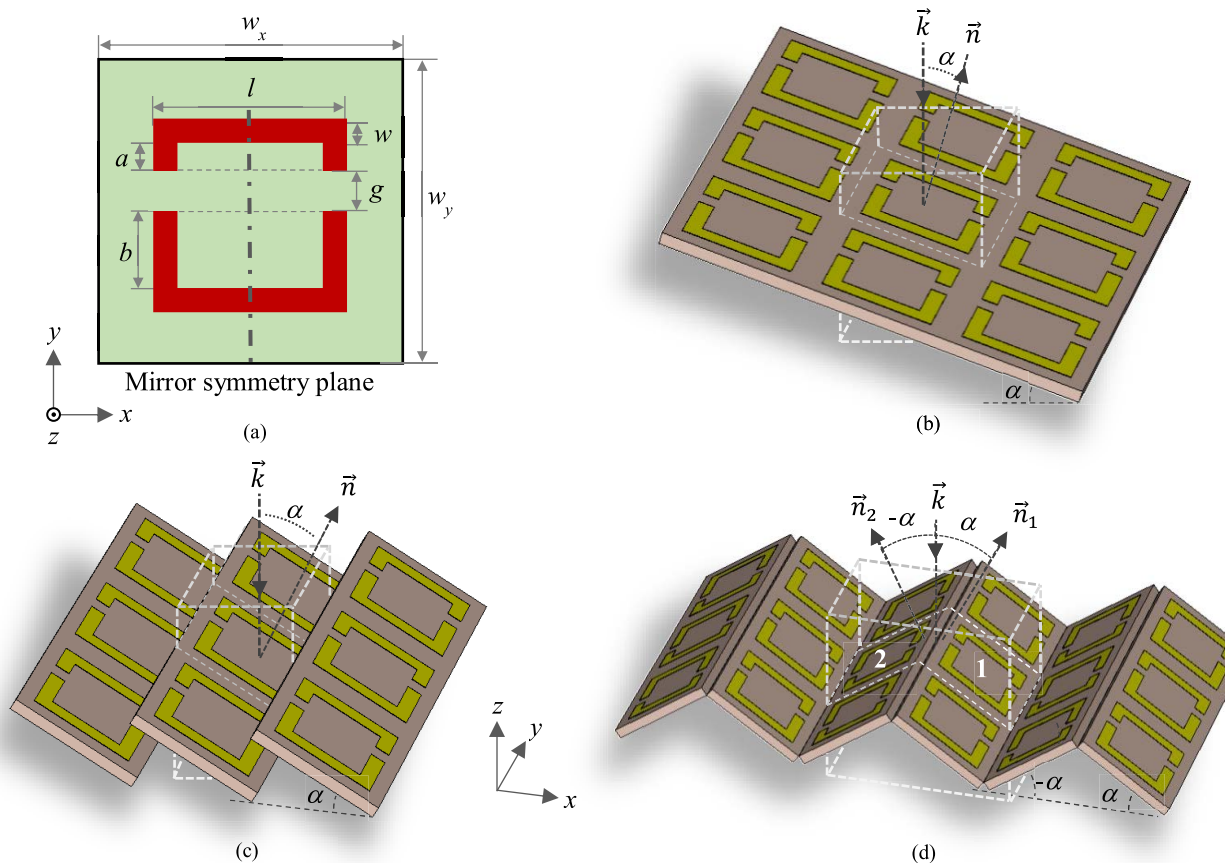


Fig. 1. (a) Schematic of the dual-gap SRR unit cell. SRR distributions: (b) planar profile, (c) Sawtooth profile, and (d) Zigzag profile.

and broadband cross-polarization conversion greater than 90%. The folding strategy was also discussed in [24], wherein CD up to 0.94 is measured with folding angles of 70° . In [25], split-ring resonators (SRRs) were distributed in an origami-based 3-D structure to provide, with a folding angle of 45° , a CD of up to 0.6. Moreover, in [26] kirigami-based CMMs were studied providing, for single-layer structures, CD values up to 0.9.

In this article, we propose two novel metamaterial structures with SRR-based unit cells distributed in sawtooth or zigzag arrangements. In these designs, the unit cells are oriented obliquely to the incident field wave vector, thus providing high extrinsic chirality. In contrast to [22], the proposed unit cell with a metal pattern on only one side of the printed circuit board (PCB) is intrinsically achiral. Through numerical and experimental characterization, we show that these nonplanar structures can present large CD values, up to 0.9, which are higher than those presented by conventional intrinsic CMMs, around 0.6 [27], [28], [29], but also by the planar distribution with oblique incidence. This improvement in the CD resides in the interaction between the unit cells, that is, mutual coupling.

The proposed structures can be used at microwave frequencies in applications involving polarization manipulation, such as filters or absorbers. Moreover, they can also be scaled to other frequency bands, for example, at Terahertz, for applications such as detection, biosensing, imaging devices,

and filters. However, at these frequencies, the manufacturing of these structures can be a technological challenge.

The remainder of this article is organized as follows. Section II presents the proposed SRR unit cell, the different unit cell distributions, and the methodology for characterizing them through simulations and measurements. The proposed distributions are characterized in detail in the corresponding subsections. Section III compares the obtained responses and analyzes the origin of the chiral behavior of these structures. Finally, Section IV presents the conclusions of this study.

II. NONPLANAR CMMs

In this section, we present nonplanar metamaterials with extrinsic chirality and compare them with the planar structures presented in previous publications [18], [19], [21]. All the structures, based on PCB technology, present unit cells formed by a square metallic ring etched on only one PCB side, as shown in Fig. 1(a). Two gaps on opposite sides of the square divide it into two square arcs, whose lengths depend on the gap length and its position along the side of the square. The geometrical parameters defining both arcs are shown in Fig. 1(a). Based on these parameters, the lengths of the top and bottom arcs are $l_{\text{arc1}} = (l + 2w + 2a)$ and $l_{\text{arc2}} = (l + 2w + 2b)$, respectively. The chosen substrate was Rogers RO4003C, with a relative permittivity of 3.55, $tg \delta = 0.0027$, and thickness 0.81 mm. The initial numerical analysis is performed using the

following geometrical parameters: $l = 7$ mm, $a = 1.2$ mm, $b = 3.36$ mm, $w = 1$ mm, and a square cell size $w_x = w_y = 9$ mm.

In the planar distribution shown in Fig. 1(b), the unit cells are uniformly distributed on a plane, with the wavevector and the metasurface normal forming an angle α . Inspired by this distribution, we explore different arrangements of unit cells to enhance the extrinsic chirality. In the first proposed structure, all the unit cells are parallel but aligned in a sawtooth arrangement [Fig. 1(c)] to obtain nonnormal incidence over the substrate. In the second distribution, the unit cells follow two different orientations, as shown in Fig. 1(d), forming a zigzag arrangement. To provide a chiral response, the SRR is designed with asymmetric arcs, $a \neq b$, to lack an inversion center and it is oriented such that the mirror symmetry plane is not perpendicular to the propagation direction, \vec{k} , and does not contain it [19].

Sections II-B–II-D analyze the three distributions with a more detailed analysis of the proposed arrangements.

A. Methodology

The proposed unit cell arrangements, shown in Fig. 1(c) and (d), were analyzed numerically and experimentally. The numerical characterization was performed with the aid of the full-wave 3-D commercial electromagnetic simulator Dassault Systems CST Microwave Studio. For this purpose, the frequency-domain solver (based on the finite element method) was applied, with unit cell boundaries in the x and y directions and open boundaries in the propagation direction z . Subsequently, both the linear (t_{xx} , t_{xy} , t_{yx} , and t_{yy}) and circular transmission coefficients (t_{++} , t_{+-} , t_{-+} , and t_{--}) were obtained. Here, t_{ab} represents the transmission coefficient of a wave with polarization type a when impinging a wave with polarization b , where a and b can be x or y for linear polarization and $+$ (RCP) or $-$ (LCP) for circular polarization.

For the experimental characterization, samples with 24×28 unit cells (sawtooth distribution) and 24×34 unit cells (zigzag distribution) were manufactured by laser etching. The measurements were performed using an Agilent E8362A PNA series network analyzer (PNA) and two standard gain horn antennas. The structure was placed between both antennas in a sampler holder formed by a metal sheet covered by an absorbent material. The metamaterial was placed in a small window at the center of the sampler holder. Thus, only the signal passing through the metamaterial reaches the receiving antenna. With this experimental setup, the linear transmission coefficients are obtained, and following (1) and (2), they can be related to the circular coefficients (an $\exp(+j\omega t)$ time harmonic convention is used).

With both types of analysis, the chiral behavior is studied in terms of CD, which is obtained as the difference between the transmittances of both eigenwaves (3)

$$t_{\pm\pm} = 0.5(t_{xx} + t_{yy} \mp j(t_{xy} - t_{yx})) \quad (1)$$

$$t_{\pm\mp} = 0.5(t_{xx} - t_{yy} \pm j(t_{xy} + t_{yx})) \quad (2)$$

$$CD = |t_{++}|^2 - |t_{--}|^2 \quad (3)$$

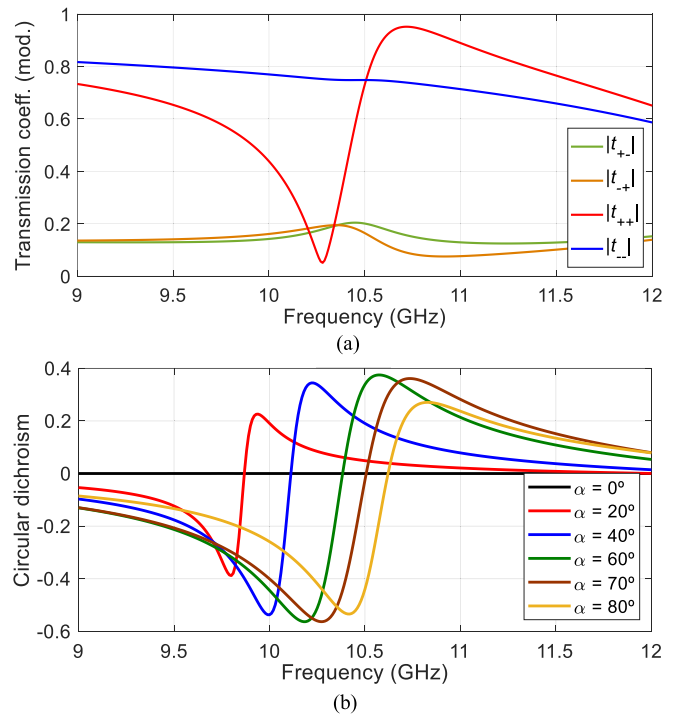


Fig. 2. SRR—Planar distribution: (a) circular transmission coefficients for $\alpha = 30^\circ$ and (b) CD for different incidence angles. Geometrical parameters (in mm): $l = 7$, $a = 1.2$, $b = 3.36$, $w = 1$, and $w_x = w_y = 9$.

B. Planar Distribution

First, as a reference for comparison with the proposed distributions, the planar arrangement shown in Fig. 2(b), with an incidence angle α from 0 to 80° , was briefly analyzed. The circular transmission coefficients for $\alpha = 30^\circ$ [Fig. 2(a)] show that, approximately at 10.2 GHz, both eigenwaves are transmitted with very different amplitudes. As shown in Fig. 2(b), the difference between the transmittances varies with α . For $\alpha = 0$, the structure is not chiral and there is no CD, as indicated in [18], [19], and [20]. As α increases, the peak of CD is higher, reaching maximum CD values of approximately -0.55 , for incidence angles between 60° and 70° . These values are consistent with those presented in [21] for a similar structure.

C. Sawtooth Distribution

The first proposed arrangement aligns the unit cells in rows along the y -axis, as shown in Fig. 1(c). Each row is tilted at a certain angle α with the rotation axis along the unit cell row center (parallel to the SRR symmetry axis). Thus, seen in the xz plane, the metamaterial exhibits a sawtooth profile. With this structure, the incident field impinges on all the unit cells obliquely at an angle α . From a geometrical point of view, the structure is 3-D chiral for all the analyzed incidence angles, from -80° to 80° , except for $\alpha = 0^\circ$, because it can be superimposed with its mirror image. This tilt angle is a key parameter on the chiral response of these extrinsically CMMs. As shown in Fig. 3(a), the absolute value of CD depends on $|\alpha|$, but its sign depends on the orientation of the tilt, that is, the sign of α . Moreover, the maximum CD value was obtained

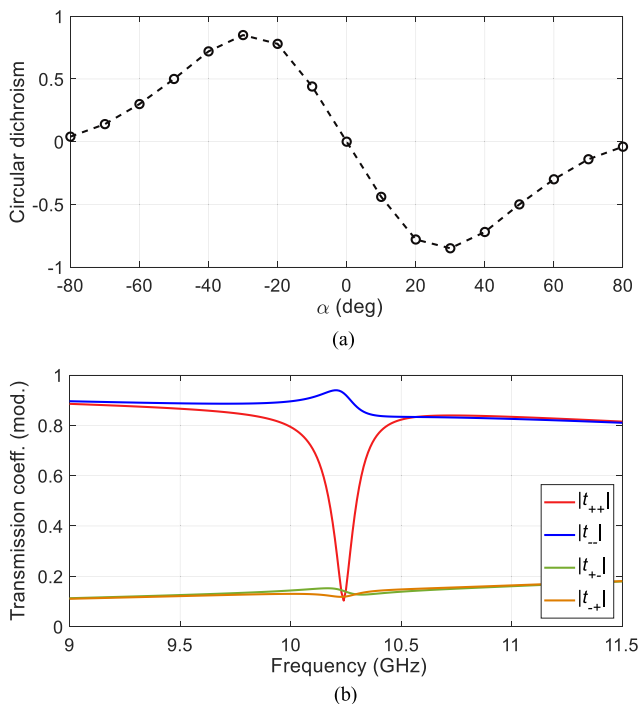


Fig. 3. Sawtooth profile: (a) CD (maximum value) as a function of α and (b) circular transmission coefficients with $\alpha = 30^\circ$. Geometrical parameters (in mm): $l = 7$, $a = 1.2$, $b = 3.36$, $w = 1$, and $w_x = w_y = 9$ ($r = 0.73$, $g = 0.44$).

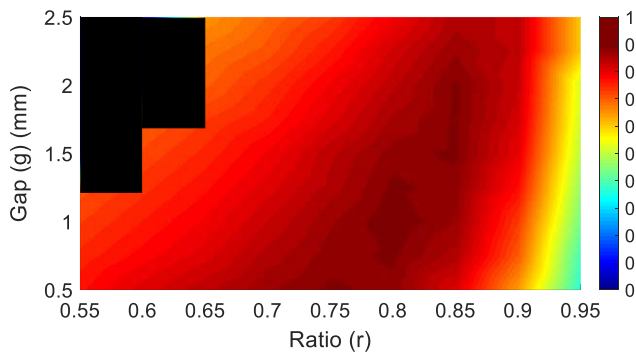
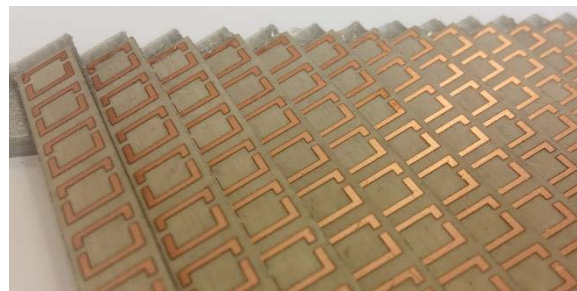


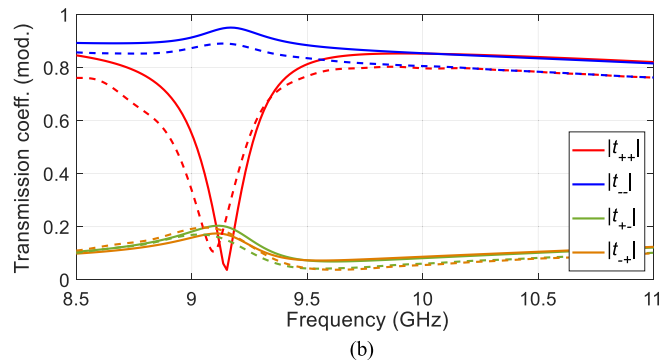
Fig. 4. Maximum CD as a function of gap length, and arc length ratio, r . Black areas represent not valid r - g combinations.

at $\alpha = \pm 30^\circ$. For $\alpha = 30^\circ$, we verify in Fig. 3(b) that the circular transmission coefficient (module) of the LCP wave is very high, approximately 0.94, whereas the other co-polar transmission coefficient is almost filtered (approximately 0.1). It is important to highlight that a sawtooth structure with a negative angle, $-\alpha$, provides the enantiomeric form of that sawtooth distribution, but with $+\alpha$. These enantiomers interchange their responses to CP waves, with $t_{\pm\pm}^{+\alpha} = t_{\mp\mp}^{-\alpha}$, and therefore, change the sign of the CD.

After determining the tilt angle with the highest CD, we now analyze how the geometrical parameters of the metallic pattern impact on the CD. Two parameters were analyzed: the gap length, g , and the ratio between the lengths of the arcs. The first governs the distance between arcs, and, as shown in Fig. 1, and is obtained as $g = l - 2w - a - b$. The second describe the symmetry of both arcs, $r = l_{\text{arc1}}/l_{\text{arc2}} = (l + 2w + 2a)/(l + 2w + 2b)$. Fig. 4 presents a color map of the maximum values



(a)



(b)

Fig. 5. (a) Photograph of the manufactured Sawtooth sample. (b) Circular transmission coefficients simulations (solid line) and measurements (dashed line) of the SRR sawtooth profile with $\alpha = 30^\circ$, $r = 0.8$, and $g = 1$ mm ($a = 1.28$ mm, $b = 2.72$ mm). The other geometrical parameters are kept constant: $l = 7$ mm, $w = 1$ mm, and $w_x = w_y = 9$ mm.

of the CD for different values of g and r . Different ratio values are obtained changing the parameters a and b while keeping l fixed, that is, modifying only the “arms” of the arcs. Black color indicates invalid gap-ratio combinations. With arc length ratios below 0.7, where the lower arc is much longer than the upper one, the structure exhibits CD values below 0.7. The highest CD values (approximately 0.9) were obtained when the arcs were similar in length, with r of approximately 0.8. In general, as r increases to 1, the gap must be longer to maintain the high CD values. Finally, for configurations with very similar arcs, r near 1, the structure tends to be symmetric (non-chiral), and the CD values fall below 0.6.

Fig. 4 presents the CD values obtained with $\alpha = 30^\circ$ for configurations with $l_{\text{arc1}} < l_{\text{arc2}}$, that is, ratios lower than 1, $r = r_0 < 1$. In these cases, $|t_{--}| > |t_{++}|$, so following (3) $\text{CD} < 0$. However, with ratios larger than one it is fulfilled that $|t_{--}| < |t_{++}|$. Moreover, for $r = 1/r_0$ the transmission coefficients t_{++} and t_{--} are interchanged, that is, $t_{\pm\pm}^{r=r_0} = t_{\mp\mp}^{r=1/r_0}$.

Based on the previous analysis, we manufactured SRR samples with a gap of 1 mm and an arc length ratio of 0.8, and assembled them in a sawtooth profile distribution, as shown in Fig. 5(a). Fig. 5(b) presents a comparison between the simulation and measurement results, showing a good agreement.

In summary, these results show that the SRR structure, when distributed in a sawtooth profile, exhibits chiral behavior with a very high CD of up to 0.9. This extrinsic chirality is controlled on the one hand by the tilt angle ($\alpha = \pm 30^\circ$ provides the best results) and on the other hand by the geometry itself, mainly by the combination gap-arc length ratio.

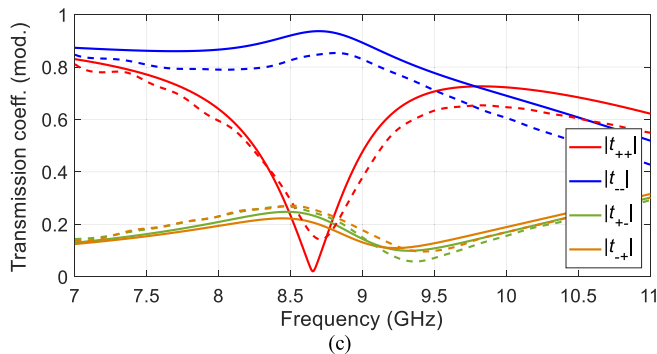
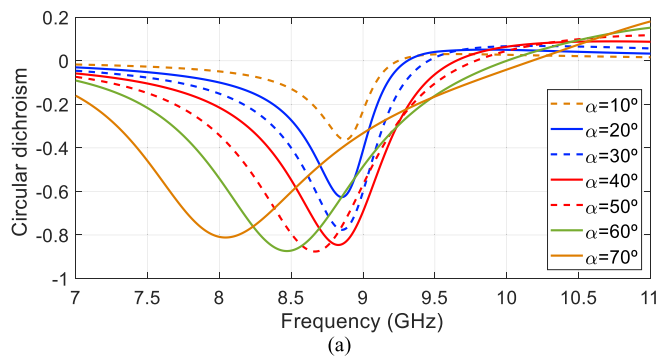


Fig. 6. Zigzag profile. (a) CD for several α values. (b) Photograph of the manufactured sample. (c) Circular transmission coefficients, simulations (solid line), and measurements (dashed line), for $\alpha = 50^\circ$.

D. Zigzag Distribution

The second proposed unit cell distribution is the zigzag assembly, as shown in Fig. 1(d). Similar to the sawtooth arrangement, this structure orders the SRRs in rows; however, in this case, these rows are rotated at the same angle but alternatively in opposite directions. The unit cell in this structure is composed of two SRR, as shown in Fig. 1(d). SRR₁ is tilted at a positive angle, $\alpha = \alpha_0$, whereas SRR₂ is tilted $\alpha = -\alpha_0$. Thus, the incident field impinges on half of the unit cell rows with α_0 and on the other half with $-\alpha_0$. Moreover, the arcs in both SRR are designed such that $r_1 = 1/r_2$, where r_1 and r_2 are the arc length ratios in SRR₁ and SRR₂ respectively. Thus, using this configuration, both faces provide the same response.

For a better comparison with the sawtooth profile, this structure was analyzed using the same geometrical parameters as in Section II-C $r_1 = 0.8$ and $g = 1$ mm ($a = 1.28$ mm, $b = 2.72$ mm), $l = 7$ mm, $w = 1$ mm, and $w_x = w_y = 9$ mm. Therefore, the analysis of the zigzag profile focuses on the impact of the incidence angle on the chiral response. Fig. 6(a) presents the CD for α angles from 10° to

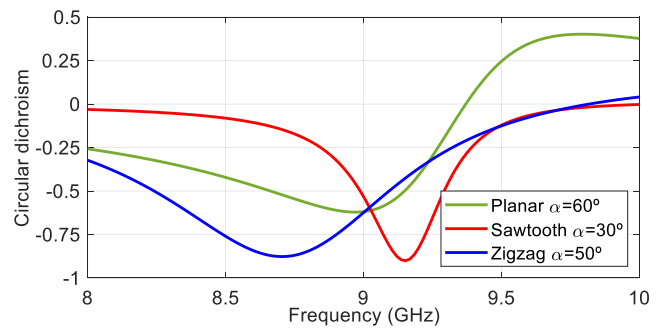


Fig. 7. Comparison of the best CD results: planar distribution, sawtooth profile, and zigzag profile. Dimensions of the SRR (in mm): $l = 7$, $w = 1$, $w_x = w_y = 9$, $\alpha = 30^\circ$, $r = 0.8$, and $g = 1$.

70° . The value $\alpha = 0^\circ$ is not presented because the structure is achiral, and thus the CD is zero. As the angle increases, the CD also increases. In the range of 0 – 40° , the CD response happens around 8.8 GHz. However, with higher α values, the CD response shifts to lower frequencies, reaching the maximum CD, approximately -0.87 , at $\alpha = 50^\circ$. It is interesting to highlight that as α increases, the bandwidth with high CD also increases. For example, for $\alpha = 50^\circ$, the $|CD| > 0.8$ in a bandwidth larger than 0.35 GHz.

We assembled the SRR samples in a zigzag profile distribution with a tilt angle of 50° [Fig. 6(b)]. The comparison between the simulated and measured circular transmission coefficients [Fig. 6(c)] shows good agreement.

III. DISCUSSION

Section II showed that the three aforementioned structures present extrinsic chirality, filtering (totally or partially) one of the eigenwaves, the RCP wave when $\alpha > 0$ or the LCP one when $\alpha < 0$, and transmitting the other one. In this section, we compare these responses by analyzing the different CD provided by each unit cell arrangement. Fig. 7 shows the best CD responses for the three unit cell distributions. To facilitate the comparison, in all cases the same geometrical parameters were used to model the SRR. Three observations were extracted from this graphical comparison. First, the responses were centered at different frequencies. Second, the proposed nonplanar distributions, zigzag and sawtooth, provided a maximum CD value of approximately 0.9, which is much higher than that of the planar distribution. Third, the zigzag profile not only provided a high CD, but also in a wider bandwidth. At this point, two questions arise: Why is the CD so high in the proposed structures and why are the results so different, even with the same geometric pattern, the SRR?

To understand the origin of this high CD, we began by analyzing the surface currents induced on the SRR. In a first analysis, we considered a large separation between SRRs to minimize the intercell coupling and focus our attention on the currents induced by the incident field. Later, the analysis will be completed by considering the interaction between the SRRs. Although this analysis was performed for the planar structure with an incidence angle of 60° , the results are extensible for the other arrangements and other angles. When impinging with a linearly polarized electric field, E_x^{inc} or E_y^{inc} , surface currents are induced on both arcs of the SRR. According

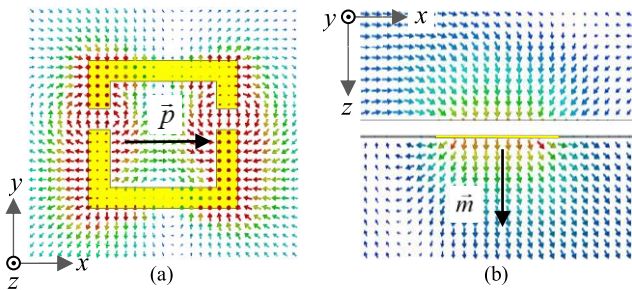


Fig. 8. (a) Electric field on the SRR plane and (b) magnetic field on the xz plane. y -Polarized incident field.

to [18], [19], and [20], these currents may be represented as a combination of two sets of currents: 1) two symmetric currents that produce an oscillating electric dipole \vec{p} , in the same plane of the unit cell and 2) two antisymmetric currents that induce an oscillating magnetic dipole \vec{m} perpendicular to the unit cell. The electric and magnetic fields shown in Fig. 8 indicate the presence of these dipoles. They appear for any α . When $\alpha = 0$, \vec{p} and \vec{m} are parallel and perpendicular, respectively, to the incidence plane; therefore, no chiral response appears. However, when $\alpha \neq 0$, both dipoles present vector components that are parallel to the incidence plane. These components provide linear cross-polar transmission linked to the chiral behavior of the structure. We refer the interested reader to [18] for a detailed analysis of the dipole moments.

It is important to highlight that the induced dipole moments generated by E_x^{inc} are similar to those generated by E_y^{inc} but $-\pi/2$ out-of-phase. Therefore, when impinging with a CP wave, defined as a combination of two linearly polarized waves, $\vec{E}_{\pm} = E_x \vec{x} \mp j E_y \vec{y}$, the dipoles generated with E_x^{inc} combined with those generated by $\mp j E_y^{\text{inc}}$, are in-phase for a LHCP wave, \vec{E}_- , and π out-of-phase for a RHCP one, \vec{E}_+ . Therefore, the high CD is originated from this constructive or destructive interference between dipole moments, filtering the RHCP wave and transmitting the orthogonal one [as observed in Figs. 3(b), 5(b), and 6(c)]. For a negative α , the dipoles generated by E_x^{inc} and E_y^{inc} are now $+\pi/2$ out-of-phase; therefore, the interference between dipoles is the opposite of the previous case: the structure filters the LHCP wave and transmits the RHCP one, that is, the sign of the CD changes [as observed in Fig. 3(a)].

Although in the three distributions the incident field induces similar surface currents on the SRRs, the different distribution of the cells provides a different interaction among neighboring SRRs and thus a different chiral response. In the planar distribution, each unit cell is edge-coupled with its adjacent SRR. Upon inspecting the electric and magnetic fields (Fig. 9(a) and (b), respectively), we observe that mutual capacitive coupling prevails between the SRR sides parallel to the y -axis because of the high charge concentration around the gaps. Meanwhile, mutual inductive coupling exists between the other SRR sides (perpendicular to the y -axis).

To illustrate this coupling Fig. 10(a) shows the lumped-element equivalent circuit model. This circuit is presented only for a better qualitative understanding of the frequency response of the structures influenced by mutual coupling. A detailed analysis of the equivalent circuit model is out of the scope of

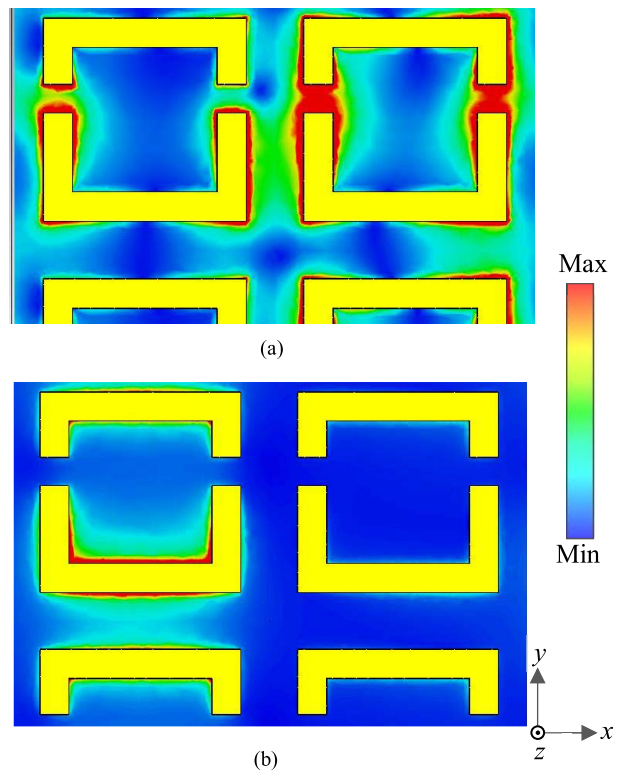


Fig. 9. (a) Electric (V/m) and (b) magnetic (A/m) fields on the xy plane with oblique E_y incidence.

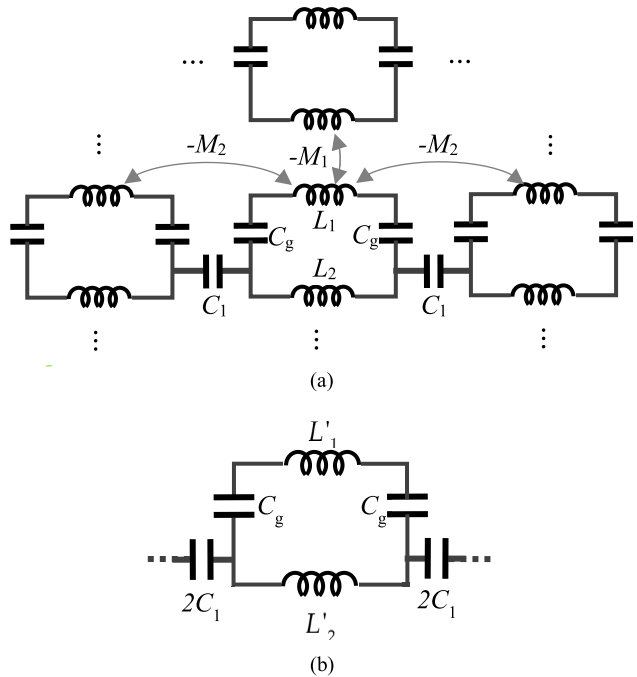


Fig. 10. (a) Lumped-element equivalent circuit model with coupling between dual split SRR. (b) Simplified circuit model of the SRR unit cell.

this study. The SRR with two splits can be modeled as two inductors L_1 and L_2 , representing the metallic arcs, and two capacitors C_g , representing the gaps. The capacitive coupling indicated previously is modeled as capacitor C_1 , while the magnetic coupling is modeled as mutual inductance $-M_1$. This mutual inductance is negative, representing differential magnetic coupling (the currents flow in opposite directions,

so the magnetic flux is counter). For the planar arrangement, the mutual inductance M_2 shown in Fig. 10(a) is zero. By modifying the circuit shown in Fig. 10(a), we obtain the equivalent circuit model of a single cell, as shown in Fig. 10(b). The inductances L'_1 and L'_2 represent the net inductances of each arm. These values are lower than those in the independent unit cell owing to the negative magnetic coupling. Without loss of generality, if we neglect the impedance of C_g , the resonance frequency f_r is defined by (4), showing a clear dependence of the intercell coupling on the resonance frequency

$$f_r = \frac{1}{2\pi\sqrt{L_{\text{Tot}}C_1}} \quad \text{with} \quad L_{\text{Tot}} = \frac{L'_1L'_2}{L'_1 + L'_2}. \quad (4)$$

The proposed non-planar arrangements present similar edgewise coupling between the adjacent cells ubicated in the same row (aligned along the y -axis). However, the interaction with the SRRs of the adjacent row changes with α . In the case of the sawtooth distribution, when the tilt angle is small, the cells are coplanar and there is a mutual capacitive edge-coupling similar to that of the planar distribution. However, as the tilt angle is increased, the SRRs tend to be broadside-coupled. In this situation, the sides of adjacent SRR are farther, that is, the distance d in Fig. 11(a) is larger. However, their mutual orientation changes from being coplanar, with $\alpha = 0$, to facing each other with $\alpha = 30^\circ$. In this orientation, there is a strong electric field between adjacent cells, as shown in Fig. 11(a), which provides an increase of the electric dipole \vec{p} , and thus, an increase of the CD. Observing the response at other frequencies, for example at 8.5 GHz as shown in Fig. 11(b), the electric field magnitude is significantly lower, reflecting a smaller capacitive coupling. Moreover, this broadside coupling between SRRs in the Sawtooth profile is also higher than the edge-coupling in the planar configuration, providing the higher CD values presented in Fig. 7. From the equivalent circuit perspective, this capacitive coupling increases C_1 , and thus the frequency response is downshifted.

In addition to the mutual capacitive coupling, this arrangement also exhibits mutual magnetic coupling between the SRRs. The dipole moment \vec{m} creates a magnetic field $\vec{B} = B_0[\sin(\alpha) \cdot \vec{a}_x + \cos(\alpha) \cdot \vec{a}_z]$. Owing to the SRRs alignment, the B_x component of this field propagates through neighboring unit cells. The corresponding magnetic flux Φ varies depending on the tilt angle α and is obtained following:

$$\Phi = B_0 \cdot A \cdot \sin^2 \alpha \quad (5)$$

where A represents the area enclosed by the SRR. According to Lenz's law, a surface current is induced on the neighboring SRR, whose flux opposes the variations in Φ . In the equivalent circuit model, Fig. 10(a), this coupling is modeled as a mutual inductance $-M_2$. As with $-M_1$, mutual coupling $-M_2$ reduces the net inductances L'_1 and L'_2 , and, following (4), shifts the resonance to higher frequencies. Moreover, it also diminishes the net surface current and thus the dipole moments, resulting in lower cross-polar transmission. Therefore, this inductive coupling represents a negative effect on the CD, even more as the tilt angle increases because Φ is higher (5).

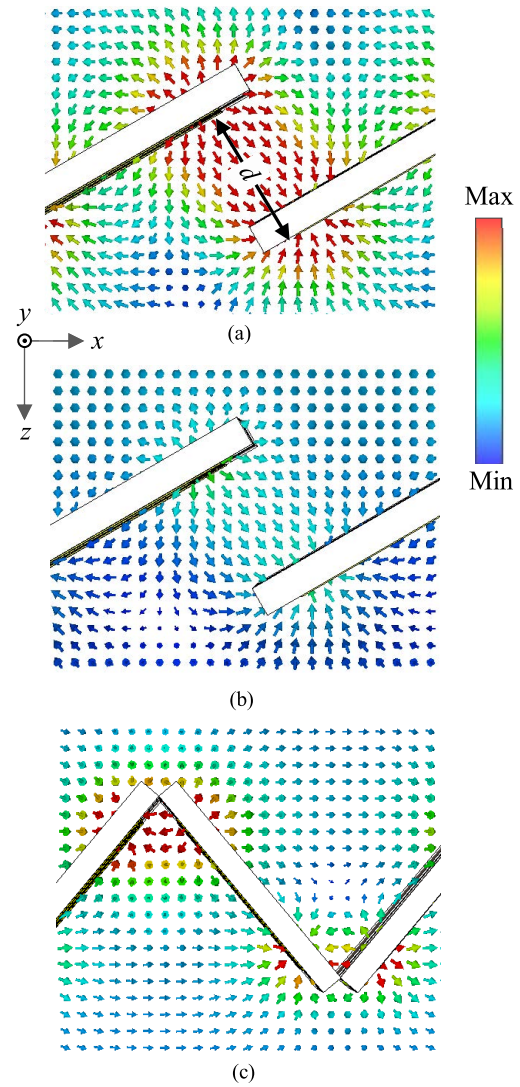


Fig. 11. Electric field distributions in xz plane for the sawtooth distribution at (a) 9.1 and (b) 8.5 GHz, and (c) zigzag distribution.

In this sawtooth distribution, the combination of both couplings provides the maximum CD values for $\alpha = 30^\circ$, due to the high electric coupling. With higher α the CD is reduced because the electric coupling is weaker (higher d and edgewise mutual orientation of the sides) and the magnetic coupling stronger.

In the case of the zigzag arrangement, it also presents inductive and capacitive coupling among neighboring SRR that can be modeled using the same equivalent circuit described for the sawtooth distribution, Fig. 10. The magnetic coupling between the cells is equal to that described for the sawtooth profile and becomes stronger as the tilt angle increases. However, in contrast to the previous structure, capacitive coupling exhibits a different behavior with respect to α . As the tilt angle increases, the SRRs are closer, and thus, the capacitive coupling becomes stronger, that is, a higher C_1 . As shown in Fig. 6(a), for $\alpha < 45^\circ$, the resonance frequency is almost constant, 8.85 GHz, because the combination of both couplings is compensated, that is, the increase in C_1 is compensated by the reduction in L_{Tot} . However, for higher angles, although

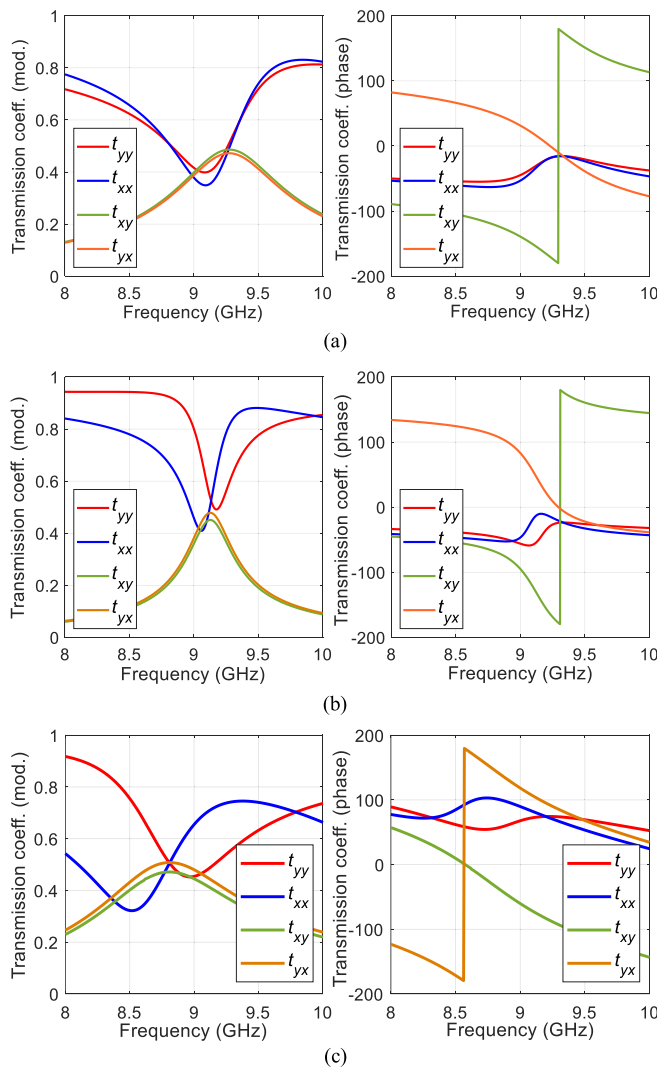


Fig. 12. Linear transmission coefficients (module and phase) for (a) planar, (b) sawtooth, and (c) zigzag profiles.

both couplings increase, the impact of capacitive coupling is stronger, resulting in a reduction in the resonance frequency (4). The zigzag arrangement exhibits CD values higher than 0.8 for α between 40° and 70° , with the highest CD value obtained for $\alpha = 50^\circ$. Fig. 11(b) presents the electric field distribution in the zigzag arrangement with that angle, showing the strong capacitive coupling between neighboring cells.

This high CD behavior can also be quantitatively characterized through the analysis of the circular transmission coefficients by means of the linear coefficients, (1) and (2). Owing to the absence of any symmetry in the structure, the four linear transmission coefficients are mutually different. However, in the three unit cell distributions, the linear transmission coefficients, represented in Fig. 12, exhibit, at the frequency of maximum CD, a similar behavior with $t_{xy} \approx -t_{yx}$ and $(t_{xx} + t_{yy})/2 \approx t_{xy} \cdot e^{j\pi/2}$. Owing to these properties, the circular cross-polar transmission coefficients $t_{\pm\mp}$ are near zero, whereas the co-polar ones are $t_{--} \approx -2jt_{xy}$ and $t_{++} \approx 0$. Thus, the CD can be approximated as $CD \approx -4|t_{xy}|^2$. The maximum values of CD obtained by this approximation,

-0.61 (planar), -0.92 (sawtooth), and -0.85 (zigzag), are in good agreement with the maximum values shown in Fig. 7, -0.62 , -0.9 , and -0.88 , respectively. Therefore, in these structures, the maximum values of the CD are directly related to the magnitude of the cross-polar transmission coefficient t_{xy} . Moreover, the sign of the CD depends on that of the phase shift between $(t_{xx} + t_{yy})/2$ and t_{xy} , which in turn, depends on that of α . Therefore, a tilt angle $\pm\alpha_0$ provides a phase shift of $\pm\pi/2$ and thus a $CD \approx \mp 4|t_{xy}|^2$.

IV. CONCLUSION

In this study, we propose different alternatives for exploiting the extrinsic chirality in single layer PCB-based structures. The metallic pattern is designed to be intrinsically achiral to evaluate only the extrinsic chirality. In a first approximation, the planar distribution exhibited chiral behavior when the incidence angle differed from zero. The highest CD values (approximately 0.62) were obtained for the high incidence angles, 60° – 70° . To improve this chiral structure, we proposed two different unit cell distributions, called sawtooth and zigzag because of the form of their profile. These structures, analyzed by simulations and measurements, provide improvements with respect to the planar distribution, yielding much higher CD values of approximately 0.9.

We have shown that in the three structures the origin of the extrinsic chiral behavior is the same: the dipole moments induced on the SRR and its constructive/destructive interference. Despite this common origin, the three structures exhibit different CD (values and frequency response). This difference in behavior is due to the geometry of the structures that produce different electric and magnetic couplings among the SRRs. The broadside capacitive coupling shown in the sawtooth and zigzag arrangements provided not only a shift in the frequency response (qualitatively reflected in the proposed equivalent circuit model) but also an improvement in the CD.

REFERENCES

- [1] L. D. Barron, *Molecular Light Scattering and Optical Activity*, 2nd ed. Cambridge, U.K.: Cambridge Univ. Press, 2004.
- [2] B. Kahr and O. Arteaga, "Arago's best paper," *ChemPhysChem*, vol. 13, no. 1, pp. 79–88, Jan. 2012, doi: [10.1002/cphc.201100660](https://doi.org/10.1002/cphc.201100660).
- [3] E. Plum et al., "Metamaterial with negative index due to chirality," *Phys. Rev. B, Condens. Matter*, vol. 79, no. 3, Jan. 2009, Art. no. 035407, doi: [10.1103/PhysRevB.79.035407](https://doi.org/10.1103/PhysRevB.79.035407).
- [4] J. B. Pendry, "A chiral route to negative refraction," *Science*, vol. 306, no. 5700, pp. 1353–1355, Nov. 2004, doi: [10.1126/science.1104467](https://doi.org/10.1126/science.1104467).
- [5] Z. Li et al., "Chiral metamaterials with negative refractive index based on four 'U' split ring resonators," *Appl. Phys. Lett.*, vol. 97, no. 8, Aug. 2010, Art. no. 081901, doi: [10.1063/1.3457448](https://doi.org/10.1063/1.3457448).
- [6] J. Li, F.-Q. Yang, and J.-F. Dong, "Design and simulation of L-shaped chiral negative refractive index structure," *Prog. Electromagn. Res.*, vol. 116, pp. 395–408, 2011, doi: [10.2528/PIER11032601](https://doi.org/10.2528/PIER11032601).
- [7] B. Wang, J. Zhou, T. Koschny, M. Kafesaki, and C. M. Soukoulis, "Chiral metamaterials: Simulations and experiments," *J. Opt. A, Pure Appl. Opt.*, vol. 11, no. 11, Nov. 2009, Art. no. 114003, doi: [10.1088/1464-4258/11/11/114003](https://doi.org/10.1088/1464-4258/11/11/114003).
- [8] R. Zhao, L. Zhang, J. Zhou, T. Koschny, and C. M. Soukoulis, "Conjugated gammadion chiral metamaterial with uniaxial optical activity and negative refractive index," *Phys. Rev. B, Condens. Matter*, vol. 83, no. 3, Jan. 2011, Art. no. 035105, doi: [10.1103/PhysRevB.83.035105](https://doi.org/10.1103/PhysRevB.83.035105).
- [9] Z. Li, M. Mutlu, and E. Ozbay, "Chiral metamaterials: From optical activity and negative refractive index to asymmetric transmission," *J. Opt.*, vol. 15, no. 2, Feb. 2013, Art. no. 023001, doi: [10.1088/2040-8978/15/2/023001](https://doi.org/10.1088/2040-8978/15/2/023001).

- [10] O. Fernández, Á. Gómez, J. Basterrechea, and A. Vegas, "Asymmetric chiral metamaterial superstrate for patch antenna polarization transformation," in *Proc. 10th Eur. Conf. Antennas Propag. (EuCAP)*, Apr. 2016, pp. 1–4, doi: [10.1109/EuCAP.2016.7481902](https://doi.org/10.1109/EuCAP.2016.7481902).
- [11] G. Kenanakis et al., "Flexible chiral metamaterials in the terahertz regime: A comparative study of various designs," *Opt. Mater. Exp.*, vol. 2, no. 12, pp. 1702–1712, Nov. 2012.
- [12] Z. Wang, F. Cheng, T. Winsor, and Y. Liu, "Optical chiral metamaterials: A review of the fundamentals, fabrication methods and applications," *Nanotechnology*, vol. 27, no. 41, Oct. 2016, Art. no. 412001, doi: [10.1088/0957-4484/27/41/412001](https://doi.org/10.1088/0957-4484/27/41/412001).
- [13] X. Ma, M. Pu, X. Li, Y. Guo, P. Gao, and X. Luo, "Meta-chirality: Fundamentals, construction and applications," *Nanomaterials*, vol. 7, no. 5, p. 116, May 2017, doi: [10.3390/nano7050116](https://doi.org/10.3390/nano7050116).
- [14] M. Malathong, A. Sonsilphong, W. Panpradit, and N. Wongkasem, "Chiral metamaterial based circularly polarized microstrip antennas," in *Proc. IEEE-APS Topical Conf. Antennas Propag. Wireless Commun.*, Sep. 2011, pp. 898–901, doi: [10.1109/APWC.2011.6046812](https://doi.org/10.1109/APWC.2011.6046812).
- [15] D. Zarifi, H. Oraizi, and M. Soleimani, "Improved performance of circularly polarized antenna using semi-planar chiral metamaterial covers," *Prog. Electromagn. Res.*, vol. 123, pp. 337–354, 2012, doi: [10.2528/PIER11110506](https://doi.org/10.2528/PIER11110506).
- [16] D. K. Rongas, S. A. Amanatiadis, A. I. Dimitriadis, and N. V. Kantartzis, "Directivity-enhanced log-spiral antenna through a chiral metamaterial superstrate," in *Proc. 7th Eur. Conf. Antennas Propag. (EuCAP)*, Apr. 2013, pp. 2079–2083.
- [17] Y. Liu, K. Song, Y. Qi, S. Gu, and X. Zhao, "Investigation of circularly polarized patch antenna with chiral metamaterial," *IEEE Antennas Wireless Propag. Lett.*, vol. 12, pp. 1359–1362, 2013, doi: [10.1109/LAWP.2013.2286191](https://doi.org/10.1109/LAWP.2013.2286191).
- [18] E. Plum, V. A. Fedotov, and N. I. Zheludev, "Optical activity in extrinsically chiral metamaterial," *Appl. Phys. Lett.*, vol. 93, no. 19, Nov. 2008, Art. no. 191911, doi: [10.1063/1.3021082](https://doi.org/10.1063/1.3021082).
- [19] E. Plum, X.-X. Liu, V. A. Fedotov, Y. Chen, D. P. Tsai, and N. I. Zheludev, "Metamaterials: Optical activity without chirality," *Phys. Rev. Lett.*, vol. 102, no. 11, Mar. 2009, Art. no. 113902, doi: [10.1103/PhysRevLett.102.113902](https://doi.org/10.1103/PhysRevLett.102.113902).
- [20] E. Plum, V. A. Fedotov, and N. I. Zheludev, "Extrinsic electromagnetic chirality in metamaterials," *J. Opt. A, Pure Appl. Opt.*, vol. 11, no. 7, Jul. 2009, Art. no. 074009, doi: [10.1088/1464-4258/11/7/074009](https://doi.org/10.1088/1464-4258/11/7/074009).
- [21] X. Hao et al., "Optically tunable extrinsic chirality of single-layer metal metasurface for terahertz wave," *Opt. Commun.*, vol. 512, Jun. 2022, Art. no. 127554, doi: [10.1016/j.optcom.2021.127554](https://doi.org/10.1016/j.optcom.2021.127554).
- [22] O. Fernández et al., "Metasurfaces with intrinsic and extrinsic chirality," in *Proc. 12th Iberian Meeting Comput. Electromagn.*, 2018, pp. 15–18.
- [23] Y. Liu, X. Huang, H. Yang, L. Hua, and Y. Lei, "Zigzag reflective multifunctional metamaterial absorber and polarization rotator with horizontal strip structure," *Phys. Scripta*, vol. 95, no. 8, Jul. 2020, Art. no. 085510, doi: [10.1088/1402-4896/aba475](https://doi.org/10.1088/1402-4896/aba475).
- [24] S. Li et al., "Reconfigurable metamaterial for chirality switching and selective intensity modulation," *Opt. Exp.*, vol. 28, no. 23, p. 34804–34811, Nov. 2020, doi: [10.1364/oe.410309](https://doi.org/10.1364/oe.410309).
- [25] Z. Wang et al., "Origami-based reconfigurable metamaterials for tunable chirality," *Adv. Mater.*, vol. 29, no. 27, Jul. 2017, Art. no. 1700412, doi: [10.1002/adma.201700412](https://doi.org/10.1002/adma.201700412).
- [26] L. Jing et al., "Kirigami metamaterials for reconfigurable toroidal circular dichroism," *NPG Asia Mater.*, vol. 10, no. 9, pp. 888–898, Sep. 2018, doi: [10.1038/s41427-018-0082-x](https://doi.org/10.1038/s41427-018-0082-x).
- [27] L. Zhou et al., "Tunable circular dichroism of stretchable chiral metamaterial," *Appl. Phys. Exp.*, vol. 13, no. 4, 2020, Art. no. 042008, doi: [10.35848/1882-0786/ab8054](https://doi.org/10.35848/1882-0786/ab8054).
- [28] Y. Cheng, Y. Nie, L. Wu, and R. Z. Gong, "Giant circular dichroism and negative refractive index of chiral metamaterial based on split-ring resonators," *Prog. Electromagn. Res.*, vol. 138, pp. 421–432, 2013, doi: [10.2528/PIER13011202](https://doi.org/10.2528/PIER13011202).
- [29] J. Shao, J. Li, Y.-H. Wang, J.-Q. Li, Z.-G. Dong, and L. Zhou, "Enhanced circular dichroism based on the dual-chiral metamaterial in terahertz regime," *Chin. Phys. B*, vol. 25, no. 5, May 2016, Art. no. 058103, doi: [10.1088/1674-1056/25/5/058103](https://doi.org/10.1088/1674-1056/25/5/058103).



Jihad Ben Yamoun received the bachelor's degree in physics and the master's degree in electronics and telecommunications from University Abdelmalek Essaadi, Tetouan, Morocco, in 2016 and 2018, respectively, where she embarked on her Ph.D. Program at the Information Technology and Systems Modeling Laboratory. Throughout her doctoral studies, she focused on enhancing the performance of Dielectric Resonator Antennas.

In February 2021, she seized a valuable opportunity to expand her practical knowledge through an internship at the University of Cantabria, Santander, Spain. Her primary focus was on delving into the properties and potential applications of chiral metamaterials. She redirected her research interests toward the captivating domain of 3-D printed antennas.



Oscar Fernández was born in Reinosa, Santander, Spain, in 1976. He received the Telecommunications Engineering and Ph.D. degrees from the University of Cantabria, Santander, in 2001 and 2007, respectively.

In 2002, he joined the Department of Communication Engineering at the University of Cantabria, where he has worked on several research projects related to radio channel characterization and metamaterials. In 2008, he became an Associate Lecturer in electronics and an Assistant Professor of RF and microwave, in 2018. His current research interests include numerical methods in electromagnetism, chiral metamaterials characterization at microwave frequencies, microwave measurements, and radio channel characterization.



Noura Aknin (Senior Member, IEEE) received the Ph.D. degree in electrical engineering in 1998 and has since established herself as a leading academic in her field.

She is a Professor of electrical and computer engineering at Abdelmalek Essaadi University, Tetouan, Morocco, a position she has held since 2000. She also serves as the Director of the Center of Doctoral Studies of Science, Technology, and Medical Science, further demonstrating her commitment to research and education. Within the university, she holds the position of the Head of the Information Technology and Modeling Systems Research Unit. She has made significant contributions to the scientific community as the Co-Founder of the IEEE Morocco Section. Furthermore, she has published numerous papers in the fields of electrical, information, and communication technologies. In addition, she has taken on the role of principal investigator for multiple national and international research projects. Her research interests primarily revolve around microwave components, mobile and wireless communications, social web, and information technologies. Her expertise in these areas has led to her involvement as a chair and scientific committee member in international conferences focused on computer and electrical sciences.

Dr. Aknin is also actively participates in various IEEE societies, showcasing her dedication to professional engagement and collaboration.



Álvaro Gómez-Gómez (Member, IEEE) was born in Santander, Spain, in 1976. He received the Licenciado en Ciencias Físicas and Ph.D. degrees from the Universidad de Cantabria, Santander, in 2000 and 2005, respectively.

From 2005 to 2008, he worked at the Departamento de Electricidad y Electrónica, Universidad de Valladolid, Valladolid, Spain. In 2010, he returned to the Departamento de Ingeniería de Comunicaciones, Universidad de Cantabria, where he became a Professor Titular de Universidad, in 2017. Along these years, he has worked on several research projects related to metamaterials. His current research interests include electromagnetic propagation in complex materials and numerical methods in electromagnetics.